 CMES, vol.96, no.3, pp.199-225, 2013

Two Dimensional Nonlocal Elasticity Analysis by Local Integral Equation Method

P.H. Wen[1], X.J. Huang[1] and M.H. Aliabadi[2]

Abstract: In this paper, a Local Integral Equation Method (LIEM) is presented for solving two-dimensional nonlocal elasticity problems . The approach is based on the Eringen's model with LIEM and the interpolation using the radial basis functions to obtain the numerical solutions for 2D problems. A weak form for the set of governing equations with a unit test function is transformed into the local integral equations. The meshless approximation technique with radial basis functions is employed for the implementation of displacements. A set of the local domain integrals is obtained in analytical form for the local elasticity and by using a standard integral scheme for the nonlocal elasticity. Three examples are presented to demonstrate the convergence and accuracy of LIEM including a rectangular plate, disk and a plate containing a circular hole subjected to a uniformly distributed displacement or tensile load. Comparisons have been made with the solutions of one dimension problems and other numerical techniques including the finite integration method, the finite/boundary element methods.

Keywords: Two dimensional nonlocal elasticity, Eringen's model, local integral equation method, weak form, radial basis functions.

1 Introduction

It is well known that the classical continuum theories such as the linear theory of elasticity are intrinsically size independent. Although the development of classical theories of linear elasticity has been quite successful for solving most engineering problems at intrinsically size independent, the need for efficient and accurate numerical method is increasingly sought for problems with nonlocal elasticity. Nowadays, it is believed that the physical nature of materials is discrete if atoms are regarded to be the basic constituents. Inter atomic forces are long range in character

[1] School of Engineering and Material Sciences, Queen Mary, University of London, London, UK, E1 4NS

[2] Department of Aeronautics, Imperial College, London, UK, SW7 2BY

while quantum mechanics, molecular dynamics, and lattice dynamics are the fundamental theory and supporting methods of approach. According to the classical theories, the elastic strains and stresses are singular at the tips of crack (dislocation) and at the corner of the notch. The continuum damage mechanics has been established to fill the gap between the classical continuum mechanics and fracture mechanics [see the works by Sudak (2003); Wang and Varadan (2008); Filiz and Aydogdu (2010); Hu et al (2008)]. A continuum model for micro-cracking in these materials leads inevitably to strain softening. It is causes a loss of positive definiteness of the elastic modulus matrix and results as an ill-posed boundary value problem, see Bazant (1976), Sandler (1984). The finite elements calculations using elasto-plastic models with yield limit degradation in the framework of the classical theory of plasticity give very different results for different discretization meshes by Bazant and Lin (1988). In other words, the finite elements results are not independent with respect to the mesh refinements and converge at infinite mesh refinement to a solution with zero energy dissipation during failure. To prevent such physically unrealistic behavior, the mathematical models with localization require that force and strain-softening region to have certain minimum finite size [see Bazant et al (1984) and Sladek et al (2003)]. A nonlocal elastic model proposed by Erigen (1983,1987) and reviewed by Altan (1989) is based on the key idea that the long-range forces are adequately described by a constitutive relation. A theory of nonlocal elasticity of bi-Helmholtz type is suited based on the Erigen's model by Lazar et al (2006). A comprehensive review on the nonlocal elasticity theory can be found in Pisano et al (2009).

In recent years, the computational mechanics community has turned its attention to so-called mesh reduction methods, see Zhang et al (2003), Zhang et al (2006), Xiaolin and Shuling (2011), Barbieri and Meo (2011), Ferronato and Pini (2010), Hao-Soo et al (2011), Khosravifard et al (2011), Li and Atluri (2008), Miers and Telles (2006), Sellountos et al (2012), Sfantos and Aliabadi (2007), Shariati et al (2010), Skouras et al (2011), Sladek et al (2013, 2006, 2010a, 2010b), Wen and Aliabadi (2009, 2007, 2008a, 2010, 2011, 2008b). These mesh reduction methods (commonly referred to as Meshless or Meshfree) have received much interest since Nayroles et al (1992)proposed the diffuse element method. Later, Belyschko et al (1994) and Liu et al (1995) proposed element-free Galerkin method and reproducing kernel particle methods, respectively. One key feature of these methods is that meshless methods do not require any grid and are hence meshless. More recently, a family of Meshless methods, based on the Local weak Petrov-Galerkin formulation (MLPGs) for arbitrary partial differential equations with moving least-square (MLS) approximation has been developed (Atluri (2004)). MLPG is reported to provide a rational basis for constructing meshless methods with a greater degree

of flexibility. Local Boundary Integral Equation method (LBIE) with moving least square and polynomial radial basis function (RBF) has been developed by Sladek et al (2006). Both methods (MLPG and LBIE) are meshless, as no domain/boundary meshes are required in these two approaches. However, Galerkin-base meshless methods, except MLGP presented by Atluri (2004) still include several awkward implementation features such as numerical integrations in the local domain. More recently, an enriched meshfree method has been developed for advanced composites [see Wen and Aliabadi (2012); Li et al (2011); Wen and Aliabadi (2010)].

In this paper, two-dimensional local boundary integral method (LIEM) is developed for the nonlocal elasticity theory with 2D Eringen's model. With the use of radial basis functions, the analytical solutions for the domain integrals in the weak form are derived for local elasticity. For the nonlocal elasticity, as there no singularity in the integral kernels, the domain integrals are obtained numerical by standard integration scheme. To compare with a high accuracy solution, two-dimension problem of a disk subjected to inner pressure load is transformed to a one-dimension problem with a second order differential equation in terms of displacement, which is solved numerically using the point collocation method by Li et al (2013). Three numerical examples demonstrate the accuracy and efficiency of LIEM.

2 Local integral equation method

A nonlocal elastic model proposed by using nonlocal elasticity by Eringen (1983, 1987) is based on the key idea that the long-range forces are adequately described by a constitutive relation of the form, for two-dimension isotropic medium, as

$$\begin{aligned}
&\sigma_{ij,j} + f_i = 0 \\
&\boldsymbol{\sigma}(\mathbf{x}) = \int_V \alpha(\mathbf{x},\mathbf{x}',l)\mathbf{D}\boldsymbol{\varepsilon}(\mathbf{x}')dV(\mathbf{x}') = \int_V \alpha(\mathbf{x},\mathbf{x}',l)\bar{\boldsymbol{\sigma}}(\mathbf{x}')dV(\mathbf{x}') \\
&\boldsymbol{\sigma} = \{\sigma_{11},\sigma_{22},\sigma_{12}\}^T,\ \boldsymbol{\varepsilon} = \{\varepsilon_{11},\varepsilon_{22},\varepsilon_{12}\}^T,\ \bar{\boldsymbol{\sigma}} = \mathbf{D}\boldsymbol{\varepsilon},\ \varepsilon_{ij} = (u_{i,j} + u_{j,i})/2
\end{aligned} \tag{1}$$

where V represents the volume of domain, f_i body forces, α a nonlocal kernel defined as the influence coefficient, l the characteristic length or influence distance; $\mathbf{x}$, $\mathbf{x}'$ are collocation and domain integration points and u_i displacements; $\boldsymbol{\sigma}$, $\bar{\boldsymbol{\sigma}}$ and $\boldsymbol{\varepsilon}$ are vectors of nonlocal stress, local stress (classical stress) and strain; $\mathbf{D}$ denotes the elastic moduli matrix. The nonlocal kernel $\alpha(\mathbf{x},\mathbf{x}',l) = \alpha(|\mathbf{x}-\mathbf{x}'|/l)$ has to satisfy the normalization condition as

$$\int_{V_\infty} \alpha\left(|\mathbf{x}-\mathbf{x}'|/l\right)dV' = 1 \tag{2}$$

in which V_∞ indicates the infinite domain embedding V.

An improvement of nonlocal elasticity model considers the nonlocal elastic material as a two-phase elastic material which includes phase 1 material complying with local elasticity and phase 2 material with nonlocal elasticity. The constitutive relation in (1) is then modified by Eringen (1983, 1987) to

$$\boldsymbol{\sigma}(\mathbf{x}) = \xi_1 \bar{\boldsymbol{\sigma}}(\mathbf{x}) + \xi_2 \int_V \alpha(\mathbf{x}, \mathbf{x}', l) \bar{\boldsymbol{\sigma}}(\mathbf{x}') dV(\mathbf{x}') \tag{3}$$

where ξ_1 and ξ_2 are portion factors and $\xi_1 + \xi_2 = 1$. By Hook's law, one has following components of stress, for two-dimensional plane-stress problem, as

$$\sigma_{11}(\mathbf{x}) = \xi_1 E' \left(\frac{\partial u_1(\mathbf{x})}{\partial x_1} + \nu \frac{\partial u_2(\mathbf{x})}{\partial x_2} \right) + \xi_2 E' \int_V \alpha(\mathbf{x}, \mathbf{x}', l) \left(\frac{\partial u_1(\mathbf{x}')}{\partial x_1'} + \nu \frac{\partial u_2(\mathbf{x}')}{\partial x_2'} \right) dV(\mathbf{x}') \tag{4a}$$

$$\sigma_{22}(\mathbf{x}) = \xi_1 E' \left(\nu \frac{\partial u_1(\mathbf{x})}{\partial x_1} + \frac{\partial u_2(\mathbf{x})}{\partial x_2} \right) + \xi_2 E' \int_V \alpha(\mathbf{x}, \mathbf{x}', l) \left(\nu \frac{\partial u_1(\mathbf{x}')}{\partial x_1'} + \frac{\partial u_2(\mathbf{x}')}{\partial x_2'} \right) dV(\mathbf{x}') \tag{4b}$$

$$\sigma_{12}(\mathbf{x}) = \xi_1 \mu \left(\frac{\partial u_1(\mathbf{x})}{\partial x_2} + \frac{\partial u_2(\mathbf{x})}{\partial x_1} \right) + \xi_2 \mu \int_V \alpha(\mathbf{x}, \mathbf{x}', l) \left(\frac{\partial u_1(\mathbf{x}')}{\partial x_2'} + \frac{\partial u_2(\mathbf{x}')}{\partial x_1'} \right) dV(\mathbf{x}') \tag{4c}$$

where $E' = E/(1-\nu^2)$, E is Young's modulus, ν is the Poisson's ratio and shear modulus $\mu = E/2(1+\nu)$. Two kinds of boundary conditions are considered for nonlocal elasticity, namely, for nonlocal traction boundary

$$\sigma_{ij} n_j = t_i^0 \tag{5}$$

and for displacement boundary

$$u_i = u_i^0 \tag{6}$$

in which u_i^0 and t_i^0 are the prescribed displacements and tractions respectively on the displacement boundary Γ_D and on the traction boundary Γ_T, and n_i is the unit normal outward to the boundary Γ.

In the nonlocal integral equation approach, the weak form of differential equation over a local integral domain Ω_s can be written, from Eq.(1), as

$$\int_{\Omega_s} (\sigma_{ij,j} + f_i) u_i^* d\Omega = 0 \tag{7}$$

where u_i^* is test function. By use of the divergence theorem, Eq.(7) above can be rewritten in a symmetric weak form as

$$\int_{\partial\Omega_s} \sigma_{ij} n_j u_i^* d\Gamma - \int_{\Omega_s} (\sigma_{ij} u_{i,j}^* - f_i u_i^*) d\Omega = 0 \tag{8}$$

If there is an intersection between the local boundary and the global boundary, a local symmetric weak form in linear elasticity may be written as

$$\int_{\Omega_s} \sigma_{ij} u_{i,j}^* d\Omega - \int_{L_s} t_i u_i^* d\Gamma - \int_{\Gamma_D} t_i u_i^* d\Gamma = \int_{\Gamma_T} t_i^0 u_i^* d\Gamma + \int_{\Omega_s} f_i u_i^* d\Omega \tag{9}$$

in which, L_s indicates the other part of the local boundary inside the local integral domain Ω_s; Γ_D is the intersection between the local boundary Γ_s and the global displacement boundary; Γ_T is a part of the traction boundary as shown in Figure 1.

The local weak forms in Eq.(8) and Eq.(9) are a starting point to derive local boundary integral equations if appropriate test functions are selected. A step functions can be used as the test functions u_i^* in each integral domain

$$u_i^*(\mathbf{x}) = \begin{cases} \varphi_i(\mathbf{x}) & \text{at } \mathbf{x} \in (\Omega_s \cup \Gamma_s) \\ 0 & \text{at } \mathbf{x} \notin \Omega_s \end{cases} . \tag{10}$$

where $\varphi_i(\mathbf{x})$ is arbitrary function. For $\varphi_i(\mathbf{x}) = 1$ and zero body force $f_i = 0$, the local weak forms Eq.(8) and Eq.(9) are transformed into simple local boundary integral equations (equilibrium of local integral domain) as

$$\int_{\partial\Omega_s} t_i d\Gamma = 0 \tag{11}$$

and

$$\int_{L_s+\Gamma_D} t_i d\Gamma = -\int_{\Gamma_T} t_i^0 d\Gamma \tag{12}$$

3 Radial basis function approximation

Consider a local domain $\partial\Omega_s$ shown in Figure 1, which is the neighbourhood of a point $\mathbf{x}$ $[= (x_1, x_2)]$ and is considered as the domain of definition of the RBF approximation for the trail function at $\mathbf{x}$ and also called as support domain to an arbitrary point $\mathbf{x}$. Generally the support domain is chosen as a circle

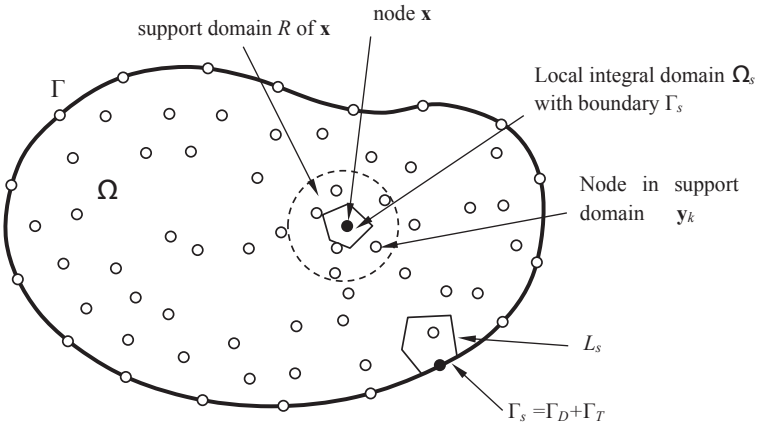

Figure 1: Arbitrary distributed node, support domain of **x**, local integral domain for weak formulation.

R centred at $\mathbf{x}$ as shown in Figure 1. To interpolate the distribution of function u in the local domain $\partial\Omega_s$ over a number of randomly distributed nodes, i.e. $\{\mathbf{y}_1, \mathbf{y}_2, ..., \mathbf{y}_K\}$, $\mathbf{y}_k[= (y_1^k, y_2^k)]$, $k = 1,2,...,K$, the approximation of function u at the point $\mathbf{x}$ can be expressed by

$$u_i(\mathbf{x}) = \sum_{k=1}^{K} R_k(\mathbf{x}, \mathbf{y}_k)\alpha_k + \sum_{t=1}^{T} P_t(\mathbf{x})\beta_t = \mathbf{R}(\mathbf{x})\boldsymbol{\alpha} + \mathbf{P}(\mathbf{x})\boldsymbol{\beta} \tag{13}$$

where $\mathbf{R}(\mathbf{x}) = \{R_1(\mathbf{x}, \mathbf{y}_1), R_2(\mathbf{x}, \mathbf{y}_2), ..., R_K(\mathbf{x}, \mathbf{y}_K)\}$ is the set of radial basis functions centred around the point $\mathbf{x}$, $\{\alpha_k\}_{k=1}^{K}$ and $\{\beta_t\}_{t=1}^{T}$ are unknowns to be determined, and $\{P_t\}_{t=1}^{T}$ is a basis for P_{T-1}, the set of d-variate polynomials of degree $\leq T-1$. The radial basis function selected multi-quadrics as

$$R_k(\mathbf{x}, \mathbf{y}_k) = \sqrt{c^2 + \left[x_1 - y_1^k\right]^2 + \left[x_2 - y_2^k\right]^2} \tag{14}$$

where c is a free parameter and along with the constraints

$$\sum_{k=1}^{K} P_t(\mathbf{y}_k)\alpha_k = 0, \quad 1 \leq t \leq T \tag{15}$$

In this paper, following polynomials are considered if $T = 6$

$$\mathbf{P} = \left\{1, x_1, x_2, x_1^2, x_1x_2, x_2^2\right\} \tag{16}$$

A set of linear equations can be written in the matrix form as

$$\mathbf{R}_0\boldsymbol{\alpha}+\mathbf{P}\boldsymbol{\beta}=\hat{\mathbf{u}},\quad \mathbf{P}^{\mathrm{T}}\boldsymbol{\alpha}=\mathbf{0} \tag{17}$$

where the coefficient matrices are defined as

$$\begin{aligned}
\mathbf{R}_0 &= \begin{bmatrix} R_1(\mathbf{y}_1,\mathbf{y}_1) & R_2(\mathbf{y}_1,\mathbf{y}_2) & \ldots & R_K(\mathbf{y}_1,\mathbf{y}_K) \\ R_1(\mathbf{y}_2,\mathbf{y}_1) & R_2(\mathbf{y}_2,\mathbf{y}_2) & \ldots & R_K(\mathbf{y}_2,\mathbf{y}_K) \\ . & . & \ldots & . \\ . & . & \ldots & . \\ . & . & \ldots & . \\ R_1(\mathbf{y}_N,\mathbf{y}_1) & R_2(\mathbf{y}_N,\mathbf{y}_2) & \ldots & R_K(\mathbf{y}_K,\mathbf{y}_K) \end{bmatrix}, \\
\mathbf{P} &= \begin{bmatrix} P_1(\mathbf{y}_1) & P_2(\mathbf{y}_1) & \ldots & P_T(\mathbf{y}_1) \\ P_1(\mathbf{y}_2) & P_2(\mathbf{y}_2) & \ldots & P_T(\mathbf{y}_2) \\ . & . & \ldots & . \\ . & . & \ldots & . \\ . & . & \ldots & . \\ P_1(\mathbf{y}_K) & P_2(\mathbf{y}_K) & \ldots & P_T(\mathbf{y}_K) \end{bmatrix}
\end{aligned} \tag{18}$$

and $\hat{\mathbf{u}}$ denotes the vector of nodal values. Solving equation (18) gives

$$\boldsymbol{\beta}=\left(\mathbf{P}^{\mathrm{T}}\mathbf{R}_0^{-1}\mathbf{P}\right)^{-1}\mathbf{P}^{\mathrm{T}}\mathbf{R}_0^{-1}\hat{\mathbf{u}},\quad \boldsymbol{\alpha}=\mathbf{R}_0^{-1}\left[\mathbf{I}-\mathbf{P}\left(\mathbf{P}^{\mathrm{T}}\mathbf{R}_0^{-1}\mathbf{P}\right)^{-1}\mathbf{P}^{\mathrm{T}}\mathbf{R}_0^{-1}\right]\hat{\mathbf{u}} \tag{19}$$

where $\mathbf{u}$ is the vector containing all the field nodal values at the L local nodes, $\mathbf{I}$ denotes the diagonal unit matrix. Substituting the coefficients α and β from (20) into (15), we can obtain the approximation of the field function, in terms of the nodal values

$$\begin{aligned}
u(\mathbf{x}) &= \left\langle \mathbf{R}(\mathbf{x})\mathbf{R}_0^{-1}\left[\mathbf{I}-\mathbf{P}\left(\mathbf{P}^{\mathrm{T}}\mathbf{R}_0^{-1}\mathbf{P}\right)^{-1}\mathbf{P}^{\mathrm{T}}\mathbf{R}_0^{-1}\right]+\mathbf{P}(\mathbf{x})\left(\mathbf{P}^{\mathrm{T}}\mathbf{R}_0^{-1}\mathbf{P}\right)^{-1}\mathbf{P}^{\mathrm{T}}\mathbf{R}_0^{-1}\right\rangle\hat{\mathbf{u}} \\
&= \sum_{i=1}^{K}\phi_i(\mathbf{x})\hat{u}_i=\boldsymbol{\Phi}(\mathbf{x})\hat{\mathbf{u}}
\end{aligned} \tag{20}$$

where $\boldsymbol{\Phi}(\mathbf{x})=\{\phi_1(\mathbf{x}),\phi_2(\mathbf{x}),...,\phi_K(\mathbf{x})\}$ is called as shape function. It is worth noticing that the shape function depends uniquely on the distribution of scattered nodes within the domain and has the Kronecker delta property.

4 Analytical forms of domain integrals

Consider a unit test function, i.e. $\varphi_i(\mathbf{x})=1$ and the local domain is enclosed by several straight lines as shown in Figure 2, therefore, the local integral equation (8)

becomes

$$\begin{aligned}\int_{\Gamma_s}\sigma_{ij}(\mathbf{x})n_j(\mathbf{x})d\Gamma(\mathbf{x}) =&\xi_1\sum_{l=1}^{L}n_j^l\int_{\Gamma_l}\bar{\sigma}_{ij}(\mathbf{x})d\Gamma(\mathbf{x})\\ &+\xi_2\sum_{l=1}^{L}n_j^l\Delta_l\int_{V}\alpha(\mathbf{x}_i,\mathbf{x}',l)\bar{\sigma}_{ij}(\mathbf{x}')dV(\mathbf{x}')\end{aligned}\tag{21}$$

where L is number of straight line for the boundary of local domain, n_j^i and Δ_i are components of normal and length of segment i of the boundary of local domain. Suppose there are M nodes both in the domain and on the boundary, $M = M_\Omega + M_T + M_D$, whereM_Ω indicates the number of nodes collocated in domain, $M_T$and M_D are numbers of nodes on the traction/displacement boundaries and consider the radial basis function interpolation in Eq.(20) and relationship between stress and strain in Eq.(1), Eq.(8) becomes

$$\begin{aligned}&\xi_1\sum_{k=1}^{K}u_1^{(k)}\sum_{l=1}^{L}\left[\sum_{i=1}^{K}\left(E'F_{1il}n_1^l+\mu F_{2il}n_2^l\right)\alpha_{ik}+\sum_{t=1}^{T}\left(E'G_{1tl}n_1^l+\mu G_{2tl}n_2^l\right)\beta_{tk}\right]\\&+\xi_2\sum_{k'=1}^{K'}u_1^{(k')}\int_V\left[\sum_{l=1}^{L}\left(E'\phi_{k',1}(\mathbf{x}')n_1^l(\mathbf{x}_l)+\mu\phi_{k',2}(\mathbf{x}')n_2^l(\mathbf{x}_l)\right)\alpha(\mathbf{x}_l,\mathbf{x}',l)\Delta_l\right]dV(\mathbf{x}')\\&+\xi_1\sum_{k=1}^{K}u_2^{(k)}\sum_{l=1}^{L}\left[\sum_{i=1}^{K}\left(\nu E'F_{2il}n_1^l+\mu F_{1il}n_2^l\right)\alpha_{ik}+\sum_{t=1}^{T}\left(\nu E'G_{2tl}n_1^l+\mu G_{1tl}n_2^l\right)\beta_{tk}\right]\\&+\xi_2\sum_{k'=1}^{K'}u_2^{(k')}\int_V\left[\sum_{l=1}^{L}\left(\nu E'\phi_{k',2}(\mathbf{x}')n_1^l(\mathbf{x}_l)+\mu\phi_{k',1}(\mathbf{x}')n_2^l(\mathbf{x}_l)\right)\alpha(\mathbf{x}_l,\mathbf{x}',l)\Delta_l\right]dV(\mathbf{x}')=0\end{aligned}\tag{22a}$$

$$\begin{aligned}&\xi_1\sum_{k=1}^{K}u_1^{(k)}\sum_{l=1}^{L}\left[\sum_{i=1}^{K}\left(\nu E'F_{1il}n_2^l+\mu F_{2il}n_1^l\right)\alpha_{ik}+\sum_{t=1}^{T}\left(\nu E'G_{1tl}n_2^l+\mu G_{2tl}n_1^l\right)\beta_{tk}\right]\\&+\xi_2\sum_{k'=1}^{K'}u_1^{(k')}\int_V\left[\sum_{l=1}^{L}\left(\nu E'\phi_{k',1}(\mathbf{x}')n_2^l(\mathbf{x}_l)+\mu\phi_{k',2}(\mathbf{x}')n_1^l(\mathbf{x}_l)\right)\alpha(\mathbf{x}_l,\mathbf{x}',l)\Delta_l\right]dV(\mathbf{x}')\\&+\xi_1\sum_{k=1}^{K}u_2^{(k)}\sum_{l=1}^{L}\left[\sum_{i=1}^{K}\left(E'F_{2il}n_2^l+\mu F_{1il}n_1^l\right)\alpha_{ik}+\sum_{t=1}^{T}\left(E'G_{2tl}n_2^l+\mu G_{1tl}n_1^l\right)\beta_{tk}\right]\\&\xi_2\sum_{k'=1}^{K'}u_2^{(k')}\int_V\left[\sum_{l=1}^{L}\left(\mu\phi_{k',1}(\mathbf{x}')n_1^l(\mathbf{x}_l)+E'\phi_{k',2}(\mathbf{x}')n_2^l(\mathbf{x}_l)\right)\alpha(\mathbf{x}_l,\mathbf{x}',l)\Delta_l\right]dV(\mathbf{x}')=0\end{aligned}\tag{22b}$$

where $k' = 1,2,...K'$ are numbers of node in the support domain centered $(\mathbf{x}')$at the local integral area $\Delta V(\mathbf{x}')$. In addition, we should introduce a grid of background as shown in Figure 2(a) to carry out domain integrals in equation (21).

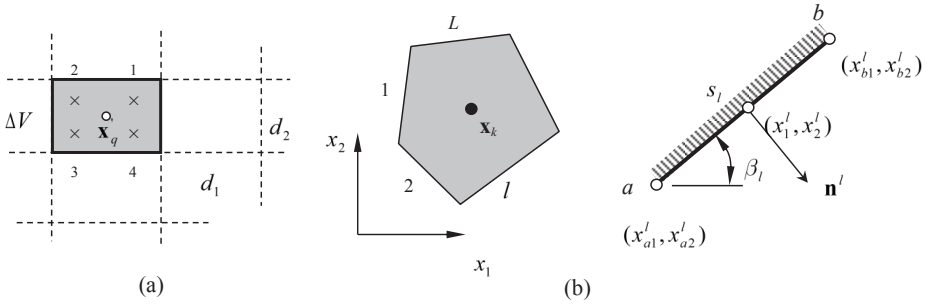

Figure 2: (a) Grid of back ground for domain integrals; (b) Local integral domain with straight boundary lines.

For arbitrary boundary shape of the local integral domain, the collocation points $\mathbf{x}_k, k = 1,2,...M_\Omega$, are shown in Figure 2(b) and boundary integrals

$$F_{jil} = \int_0^{s_l} \frac{\partial R_i}{\partial x_j} ds,\ G_{jtl} = \int_0^{s_l} \frac{\partial P_t}{\partial x_j} ds \tag{23}$$

Consider $n_1^l = \sin\beta_l, n_2^l = -\cos\beta_l$, we have solutions in closed form by Wen and Aliabadi (2013)

$$\begin{aligned}
F_{1il} &= (r_2 - r_1)\cos\beta_l - [(x_{a1}^l - y_1^i)\sin\beta_l - (x_{a2}^l - y_2^i)\cos\beta_l]\sin\beta_l \ln\frac{d_1}{d_2} \\
F_{2il} &= (r_2 - r_1)\sin\beta_l - [(x_{a2}^l - y_2^i)\cos\beta_l - (x_{a1}^l - y_1^i)\sin\beta_l]\cos\beta_l \ln\frac{d_1}{d_2}
\end{aligned}$$

$$\begin{aligned}
r_1 &= \sqrt{c^2 + (x_{a1}^l - y_1^i)^2 + (x_{a2}^l - y_2^i)^2} \\
r_2 &= \sqrt{c^2 + (x_{b1}^l - y_1^i)^2 + (x_{b2}^l - y_2^i)^2} \\
d_1 &= (x_{a1}^l - y_1^i)\cos\beta_l + (x_{a2}^l - y_2^i)\sin\beta_l + r_1 \\
d_2 &= (x_{b1}^l - y_1^i)\cos\beta_l + (x_{b2}^l - y_2^i)\sin\beta_l + r_2
\end{aligned} \tag{24}$$

If $T = 6$, from Eq.(16), one has

$$G_{11l} = G_{13l} = G_{16l} = 0$$

$$G_{12l} = s, G_{14l} = 2x_{a1}s + s^2\cos\beta_i, \quad G_{15l} = x_{a2}s + \frac{s^2\sin\beta_i}{2}$$

$$G_{21l} = G_{22l} = G_{24l} = 0,$$

$$G_{23l} = s, G_{25l} = x_{a1}s + \frac{s^2\cos\beta_i}{2}, G_{26l} = 2x_{a2}s + s^2\sin\beta_i$$
$$s = \sqrt{(x^i_{b1} - x^i_{a1})^2 + (x^i_{b2} - x^i_{a2})^2}. \tag{25}$$

For all domain integrals, four-point standard integral scheme is adopted in computation. Then Eqs (22a) and (22b) above are rewritten as

$$\begin{aligned}
&\xi_1 \sum_{k=1}^{K} u_1^{(k)} \sum_{l=1}^{L} \left[\sum_{i=1}^{K} \left(E' F_{1il} n_1^l + \mu F_{2il} n_2^l \right) \alpha_{ik} + \sum_{t=1}^{T} \left(E' G_{1tl} n_1^l + \mu G_{2tl} n_2^l \right) \beta_{tk} \right] \\
&+ \xi_2 \sum_{k'=1}^{K'} u_1^{(k')} \sum_{q=1}^{V} \sum_{p=1}^{4} \sum_{l=1}^{L} \left(E' \phi_{k',1}(\mathbf{x}'_{qp}) n_1^l(\mathbf{x}_l) + \mu \phi_{k',2}(\mathbf{x}'_{qp}) n_2^l(\mathbf{x}_l) \right) \alpha(\mathbf{x}_l, \mathbf{x}'_{qp}, l) \Delta_l w_p \Delta V_q \\
&+ \xi_1 \sum_{k=1}^{K} u_2^{(k)} \sum_{l=1}^{L} \left[\sum_{i=1}^{K} \left(\nu E' F_{2il} n_1^l + \mu F_{1il} n_2^l \right) \alpha_{ik} + \sum_{t=1}^{T} \left(\nu E' G_{2tl} n_1^l + \mu G_{1tl} n_2^l \right) \beta_{tk} \right] \\
&+ \xi_2 \sum_{k'=1}^{K'} u_2^{(k')} \sum_{q=1}^{V} \sum_{p=1}^{4} \sum_{l=1}^{L} \left(\nu E' \phi_{k',2}(\mathbf{x}'_{qp}) n_1^l(\mathbf{x}_l) + \mu \phi_{k',1}(\mathbf{x}'_{qp}) n_2^l(\mathbf{x}_l) \right) \alpha(\mathbf{x}_l, \mathbf{x}'_{qp}, l) \Delta_l w_p \Delta V_q = 0
\end{aligned} \tag{26a}$$

$$\begin{aligned}
&\xi_1 \sum_{k=1}^{K} u_1^{(k)} \sum_{l=1}^{L} \left[\sum_{i=1}^{K} \left(\nu E' F_{1il} n_2^l + \mu F_{2il} n_1^l \right) \alpha_{ik} + \sum_{t=1}^{T} \left(\nu E' G_{1tl} n_2^l + \mu G_{2tl} n_1^l \right) \beta_{tk} \right] \\
&+ \xi_2 \sum_{k'=1}^{K'} u_1^{(k')} \sum_{q=1}^{V} \sum_{p=1}^{4} \sum_{l=1}^{L} \left(\nu E' \phi_{k',1}(\mathbf{x}'_p) n_2^l(\mathbf{x}_l) + \mu \phi_{k',2}(\mathbf{x}'_p) n_1^l(\mathbf{x}_l) \right) \alpha(\mathbf{x}_l, \mathbf{x}'_p, l) \Delta_l w_p \Delta V_q \\
&+ \xi_1 \sum_{k=1}^{K} u_2^{(k)} \sum_{l=1}^{L} \left[\sum_{i=1}^{K} \left(E' F_{2il} n_2^l + \mu F_{1il} n_1^l \right) \alpha_{ik} + \sum_{t=1}^{T} \left(E' G_{2tl} n_2^l + \mu G_{1tl} n_1^l \right) \beta_{tk} \right] \\
&\xi_2 \sum_{k'=1}^{K'} u_2^{(k')} \sum_{q=1}^{V} \sum_{p=1}^{4} \sum_{l=1}^{L} \left(\mu \phi_{k',1}(\mathbf{x}'_p) n_1^l(\mathbf{x}_l) + E' \phi_{k',2}(\mathbf{x}'_p) n_2^l(\mathbf{x}_l) \right) \alpha(\mathbf{x}_l, \mathbf{x}'_p, l) \Delta_l w_p \Delta V_q = 0
\end{aligned} \tag{26b}$$

where V in the summation above indicates the number of total rectangular segments of whole integral domain using a background grid, $\mathbf{x}'_{qp} = \mathbf{x}'_q + \mathbf{x}'_p$. For a rectangular area of ΔV, one has

$$\begin{aligned}
&\mathbf{x}'_1 = (d_1/2\sqrt{3}, d_2/2\sqrt{3}),\ \mathbf{x}'_2 = (-d_1/2\sqrt{3}, d_2/2\sqrt{3}), \\
&\mathbf{x}'_3 = (-d_1/2\sqrt{3},\ -d_2/2\sqrt{3}),\ \mathbf{x}'_4 = (d_1/2\sqrt{3},\ -d_2/2\sqrt{3}), \\
&w_p = 1/4,\ \Delta V_q = d_1 d_2
\end{aligned} \tag{27}$$

A part from the collocation points in the domain, we need to consider the traction/displacement boundary conditions for the nodes collocated on the boundary. For the nodes on the traction boundary, Eq.(11) should be introduced

$$\int_{\Gamma-\Gamma_T} t_i d\Gamma = -\int_{\Gamma_T} t_i^0 d\Gamma \quad \text{for} \quad \mathbf{x}_k \; k = 1,2,...,M_T \tag{28}$$

For the displacement boundary nodes, we can introduce the displacement equation directly, i.e. $u_i(\mathbf{x}_k) = u_i^0, k = 1,2,...M_D$. Therefore, there are $2 \times (M_\Omega + M_T + M_D)$ linear algebraic equations in total to determine the same number unknowns of displacements either in the domain or on the traction boundary.

To observe the accuracy and convergence of the local integral equation method, four different shapes as shown in Figure 4 for the local integral domain, L=3, 4, 8 and 128, were studied by Wen and Aliabadi (2013). The accuracy was demonstrated with several complicated elsato-static and elasto-dynamic problems and the selections for free parameters such as c in the radial bases function, D local integral domain side, r_0 radius of the local support domain. In this paper, we use: $c = \Delta_{\min}$, $D = \Delta_{\min}$ and number of integration $L = 4$, where $\Delta_{\min}$ indicates the minimum distance between the nodes in the local integral domain. The support domain is selected as a circle of radius r_0 centered at field point $\mathbf{x}$, which is determined such that the minimum number of nodes in the support domain $K \geq K_0$, here the number K_0 is selected to be 12 for all examples in the following sections. In addition, a grid of background as shown in Figure 2(a) $(d_1 \times d_2)$ is introduced to carry out all domain integrals in Eq.(21). For two-dimension problem, the nonlocal influence function is selected as $\alpha(\mathbf{x},\mathbf{x}',l) = \lambda_0 \exp(-|\mathbf{x}-\mathbf{x}'|/l)$ in this paper, where $\lambda_0 = 1/2\pi l^2$, l is the characteristic length selected according to the range and sensitivity of the physical phenomena.

5 Nonlocal elasticity for disk

To verify the proposed method to two-dimensional nonlocal elasticity, we can compare the numerical results with either the finite element method or the finite difference method. For the polar symmetric problems such as a disk (2D) or a sphere (3D), it can be simplified to a one-dimensional problem and the solution can be obtained accurately by using either the finite difference method or the finite integration method by Li et al (2013).

Consider a disk of outer radius r_b and inner radius r_a as shown in Figure 3 subjected to pressure load p_b on outer surface and p_a on inner surface. As the polar symmetry, the strains in the disk are function of radius r only and written as

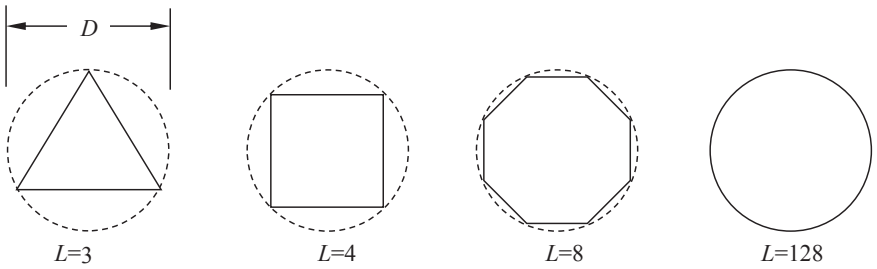

Figure 3: Different shapes of local integral domain and character parameter D.

$$\varepsilon_r = \frac{du}{dr},\ \varepsilon_\theta = \frac{u}{r} \tag{29}$$

and equilibrium equation is

$$\frac{d\sigma_r}{dr} + \frac{\sigma_r - \sigma_\theta}{r} = 0 \tag{30}$$

The local stresses in the Cartesian coordinate system at field point **x**' are

$$\begin{aligned}
\bar{\sigma}_{11}(\rho,\theta) &= \bar{\sigma}_r(\rho)\cos^2\theta + \bar{\sigma}_\theta(\rho)\sin^2\theta \\
\bar{\sigma}_{22}(\rho,\theta) &= \bar{\sigma}_r(\rho)\sin^2\theta + \bar{\sigma}_\theta(\rho)\cos^2\theta \\
\bar{\sigma}_{12}(\rho,\theta) &= (\bar{\sigma}_r - \bar{\sigma}_\theta)\sin\theta\cos\theta
\end{aligned} \tag{31}$$

Then the constitutive relation for the nonlocal elasticity theory with two dimensional Eringen's model can be written, in the case of plane stress as shown in Figure 4(b), as

$$\begin{aligned}
&\sigma_r(\mathbf{x}) = \sigma_{11}(r,0) = \xi_1\bar{\sigma}_r(r) + \xi_2\int_V \alpha(\mathbf{x},\mathbf{x}',l)\bar{\sigma}_{11}(\rho,\theta)dV(\mathbf{x}') \\
&= \xi_1 E'\left(\frac{du(\mathbf{x})}{dr} + \nu\frac{u(\mathbf{x})}{r}\right) \\
&+ \xi_2 E'\int_V \alpha(\mathbf{x},\mathbf{x}',l)\left[\left(\frac{du(\mathbf{x}')}{d\rho} + \nu\frac{u(\mathbf{x}')}{\rho}\right)\cos^2\theta + \left(\nu\frac{du(\mathbf{x}')}{d\rho} + \frac{u(\mathbf{x}')}{\rho}\right)\sin^2\theta\right]dV(\mathbf{x}')
\end{aligned} \tag{32a}$$

$$\sigma_\theta(\mathbf{x}) = \sigma_{22}(r,0) = \xi_1 \bar{\sigma}_\theta(r) + \xi_2 \int_V \alpha(\mathbf{x},\mathbf{x}',l)\bar{\sigma}_{22}(\rho,\theta)dV(\mathbf{x}')$$
$$= \xi_1 E' \left(\nu \frac{du(\mathbf{x})}{dr} + \frac{u(\mathbf{x})}{r}\right)$$
$$+ \xi_2 E' \int_V \alpha(\mathbf{x},\mathbf{x}',l) \left[\left(\frac{du(\mathbf{x}')}{d\rho} + \nu\frac{u(\mathbf{x}')}{\rho}\right)\sin^2\theta + \left(\nu\frac{du(\mathbf{x}')}{d\rho} + \frac{u(\mathbf{x}')}{\rho}\right)\cos^2\theta\right] dV(\mathbf{x}') \tag{32b}$$

and

$$\sigma_{r\theta}(\mathbf{x}) = 0. \tag{32c}$$

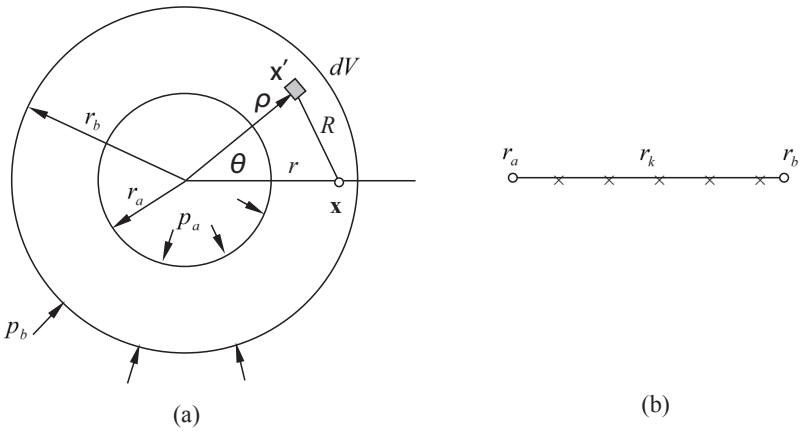

Figure 4: Disk ring under pressure load. (a) polar coordinate; (b) one dimension nodal distribution.

For the influence function $\alpha(\mathbf{x},\mathbf{x}',l) = e^{-|\mathbf{x}'-\mathbf{x}|/l}/2\pi l^2$, substituting Eq.(32) into Eq.(30) yields a one dimensional integral equation as

$$\frac{d^2u}{dr^2} + \frac{1}{r}\frac{du}{dr} - \frac{u}{r^2} - \frac{\xi_2}{2\pi l^3 \xi_1}\int_0^{2\pi}\int_{r_a}^{r_b} e^{-R/l}\frac{\partial R}{\partial r}\left[\left(\frac{du}{d\rho} + \nu\frac{u}{\rho}\right)\cos^2\theta + \left(\nu\frac{du}{d\rho} + \frac{u}{\rho}\right)\sin^2\theta\right]\rho d\rho d\theta$$
$$+ \frac{\xi_2(1-\nu)}{2\pi l^2 \xi_1 r}\int_0^{2\pi}\int_{r_a}^{r_b} e^{-R/l}\left(\frac{du}{d\rho} - \frac{u}{\rho}\right)\left(\cos^2\theta - \sin^2\theta\right)\rho d\rho d\theta = 0 \tag{33}$$

where

$$R=\sqrt{r^2+\rho^2-2r\rho\cos\theta} \quad \text{and} \quad \frac{\partial R}{\partial r}=\frac{r-\rho\cos\theta}{R}.$$

By using of shape function in Eq.(20), one has

$$u(r)=\sum_{i=1}^{N}\phi_i(r)u^i \tag{34}$$

where u^i are nodal values. Eq. (33) becomes

$$\begin{aligned}
&\sum_{i=1}^{N}\left(\phi_{i,rr}(r)+\frac{\phi_{i,r}(r)}{r}-\frac{\phi_i(r)}{r^2}\right)u^i \\
&-\frac{\xi_2}{2\pi l^3\xi_1}\sum_{i=1}^{N}u^i\int_0^{2\pi}\int_{r_a}^{r_b}e^{-R/l}\frac{r-\rho\cos\theta}{R}\left[\left(\phi_{i,\rho}(\rho)+\nu\frac{\phi_i(\rho)}{\rho}\right)\cos^2\theta+\right. \\
&\left.\left(\nu\phi_{i,\rho}(\rho)+\frac{\phi_i(\rho)}{\rho}\right)\sin^2\theta\right]\rho d\rho d\theta \\
&+\frac{\xi_2(1-\nu)}{2\pi l^2\xi_1 r}\sum_{i=1}^{N}u^i\int_0^{2\pi}\int_{r_a}^{r_b}e^{-R/l}\left(\phi_{i,\rho}(\rho)-\frac{\phi_i(\rho)}{\rho}\right)\rho d\rho d\theta=0
\end{aligned} \tag{35}$$

where the collocation point r is selected, for the uniformly distributed collocation points in the disk, to be $r=r_a+k(r_b-r_a)/N,\ \ k=1,2,...,N-1\ (N\geq 2)$. For the inner and outer surfaces of disk, we have $\sigma_r(r_a)=p_a$ and $\sigma_r(r_b)=p_b$, i.e.

$$\begin{aligned}
&\xi_1E'\sum_{i=1}^{N}u^i\left(\phi_{i,r}(r_1)+\nu\frac{\phi_i(r_a)}{r_a}\right)+\xi_2E'\sum_{i=1}^{N}u^i\int_0^{2\pi}\int_{r_a}^{r_b}\alpha(r_a,\mathbf{x}',l)\left[\left(\phi_{i,\rho}(\rho)+\nu\frac{\phi_i(\rho)}{\rho}\right)\cos^2\theta+\right. \\
&\left.\left(\nu\phi_{i,\rho}(\rho)+\frac{\phi_i(\rho)}{\rho}\right)\sin^2\theta\right]\rho d\rho d\theta=p_a
\end{aligned} \tag{36a}$$

$$\begin{aligned}
&\xi_1E'\sum_{i=1}^{N}u^i\left(\phi_{i,r}(r_2)+\nu\frac{\phi_i(r_b)}{r_b}\right)+\xi_2E'\sum_{i=1}^{N}u^i\int_0^{2\pi}\int_{r_a}^{r_b}\alpha(r_b,\mathbf{x}',l)\left[\left(\phi_{i,\rho}(\rho)+\nu\frac{\phi_i(\rho)}{\rho}\right)\cos^2\theta+\right. \\
&\left.\left(\nu\phi_{i,\rho}(\rho)+\frac{\phi_i(\rho)}{\rho}\right)\sin^2\theta\right]\rho d\rho d\theta=p_b
\end{aligned} \tag{36b}$$

There are $N+1$ algebraic linear equations including (N-1) equilibrium equations in Eq.(35) and two boundary conditions in Eq.(36) above to be used to determine $N+1$ nodal displacementsu^i.

6 Numerical examples

In this section, the application of the meshless local integral equation method for two-dimensional nonlocal elasticity static problems is demonstrated by three examples. All free parameters including c, D and r_0 are selected as discussed in chapter 4. A square plate subjected to uniform tensile load and uniform displacement is observed in example 6.1. One-dimensional solutions by Li et al (2013) and two dimensional solution of NL-FEM by Pisano et al (2009) are compared. A disk subjected to inner pressure is analysed in example 6.2 and the solutions both for 2D and 1D numerical processes are compared. Finally, a square plate with a circle hole is considered in example 6.3 to demonstrate the application of LIEM to a general problem.

6.1 A square plate under tensile load

First, we consider a square plate of side $a = 5$cm subjected to a uniformly distributed force along two sides $\left(t_1^0 = \pm\sigma_0\right)$ as shown in Figure 5(a). Young's modulus is one unit and and Poisson ratio $\nu = 0$. In this case, the accurate solution for one-dimension bar as observed by Li et al (2013) can be used for comparison. The dimensionless parameter $\xi_1 = \xi_2 = 0.5$ and the characteristic length $l/a = 0.1$. Two types of uniform distribution of node are considered, i.e. the number of total node $N_1 \times N_2 = 11 \times 11$ and 21×21 respectively.

To demonstrate the convergence of this method, the variation of the normalized local stress $\bar{\sigma}_{22}(x_1) = E\varepsilon_{22}/\sigma_0$ at $x_2 = a/2$ by both the local integral equation method (2D) and the finite integration method by Li et al (2013) (1D) are plotted in Figure 5. It is illustrated that the boundary effect for 2D nonlocal elasticity theory is significant as same as 1D problem. As expected, the results given by LIEM are convergent for two densities of node distribution and hence the solution for the fine grid of node is closer to that for one dimensional case too. Both normalized solutions tend to one unit at the middle of the plate/bar. However, these two solutions, i.e. two-dimension and one-dimension, should not be expected to be the same as the different influence functions $\alpha(\mathbf{x}, \mathbf{x}', l)$.

Consider the same geometry of the plate above fixed along the edge at $x_1 = 0$ and a uniform distribution of displacement $u_1^0 = 0.001$cm along the edge $x_1 = 5$ (see Pisano (2009)) as shown in Figure 4(b). In this case, Young's modulus $E = 2.1 \times 10^6 N/cm^2$, Poisson ratio $\nu = 0.2$, characteristic length $l = 0.1$cm and parameter $\xi_1 = 0.5$. A uniform distribution of node (21×21) is considered and all other free parameters are the same as in example above. Figure 5 shows the distribution of strain ε_{11} versus x_1 at $x_2 = 0.019$cm and $x_2 = 2.519$cm respectively. The results by Pisano et al (2009) using NL-FEM are presented in Figure 5 for comparison.

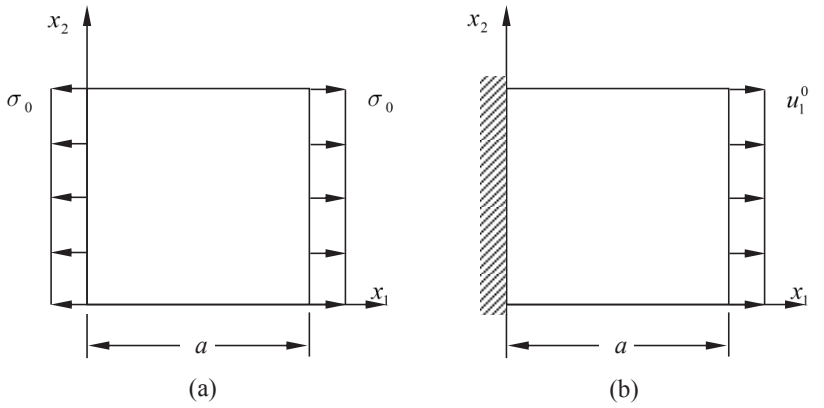

Figure 5: Square plate. (a) under tensile load; (b) uniform displacement.

6.2 A disk under internal pressure load

A disk under an internal pressure load is analysed as shown in Figure 7(a). Poisson ratio $\nu = 0.3$ and dimensions $a = 1$cm and $b = 2$cm. Due to the symmetry, one quarter of the disk is studied by using LIEM in this example. However, in the domain integral in the governor equation, the contributions to the strain from the whole disk must be taken into account as shown in Figure 10(a). The boundary condition is described as

$$\begin{aligned}
&t_1^0 = -p_a \cos\varphi,\ t_2^0 = -p_a \sin\varphi \quad \text{for} \quad \sqrt{x_1^2 + x_2^2} = 1\text{cm};\\
&t_1^0 = 0,\ t_2^0 = 0 \quad \text{for} \quad \sqrt{x_1^2 + x_2^2} = 2\text{cm};\\
&t_1^0 = 0,\ u_2^0 = 0 \quad \text{for} \quad x_2 = 0;\\
&t_2^0 = 0,\ u_1^0 = 0 \quad \text{for} \quad x_1 = 0.
\end{aligned} \tag{37}$$

The node distribution is shown in Figure 7(b), here the total number of node $N = 1039$. Again, all free parameters c, D and r_0 are selected as same as example above. The number of grid as shown in Figure 2(a) is selected as (41×41). The normalised strains $E\varepsilon_{11}(x_1,0)/p_a$ and $E\varepsilon_{22}(x_1,0)/p_a$ along the axis x are plotted in Figures from 7 to 10 for different parameters l and ξ_1. One dimensional solution with high accuracy by using the point collocation method is reported in the same figures for comparison. Obviously good agreement between these solutions has been achieved.

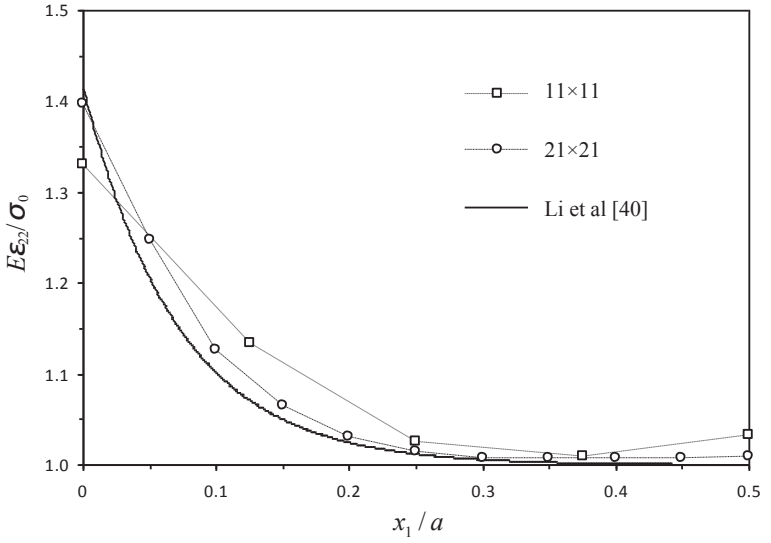

Figure 6: Normalised nonlocal stress $\bar{\sigma}_{22} = E\varepsilon_{22}/\sigma_0$ at $x_2 = a/2$ for different densities of node distribution.

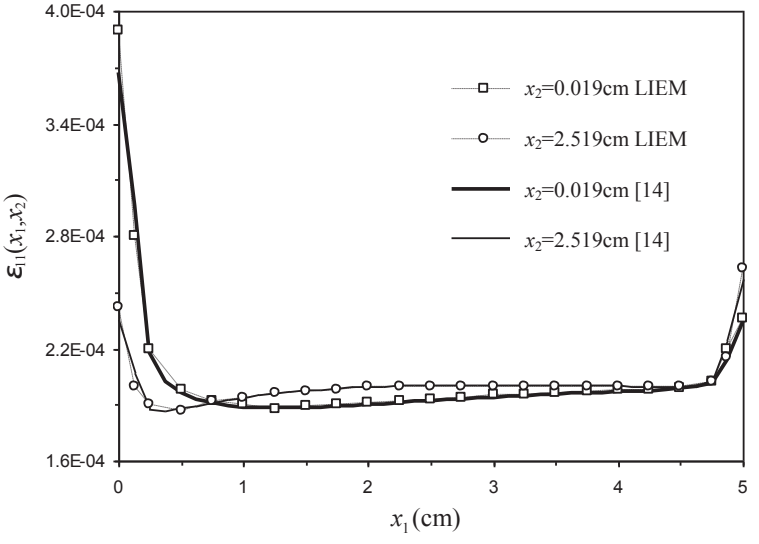

Figure 7: Distribution of strain ε_{11} versus x_1 of a square plate under uniform tensile load given by LIEM and NL-FEM [14].

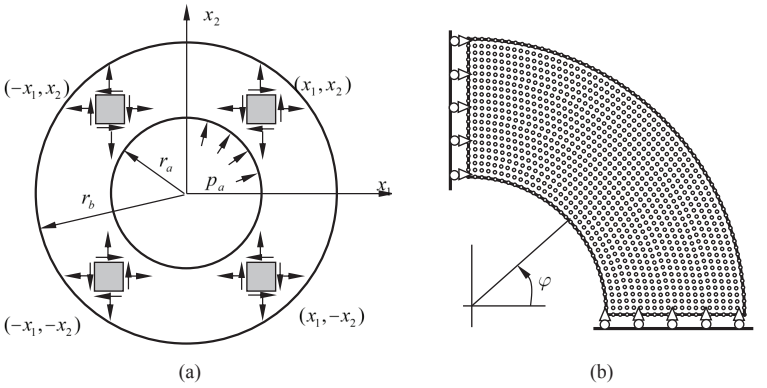

Figure 8: A disk under pressure load. (a): superposition for simplification; (b) nodal distribution in a quarter of disk and boundary conditions.

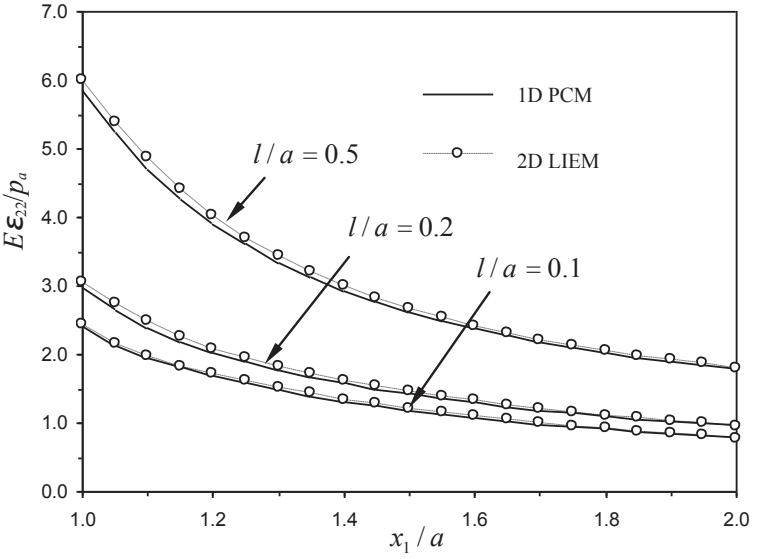

Figure 9: Distribution of the normalized strain $E\varepsilon_{22}/p_a$ for different parameter l/a when the characteristic length $\xi_1 = 0.1$.

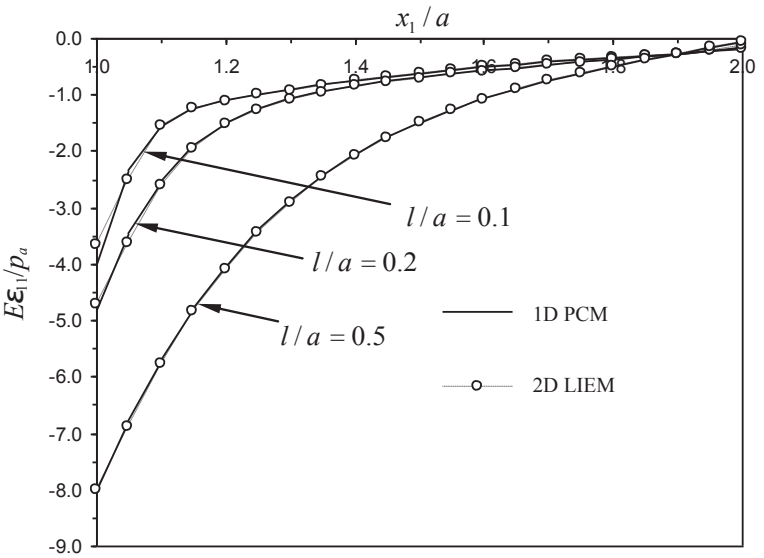

Figure 10: Distribution of the normalized strain $E\varepsilon_{11}/p_a$ for different parameter l/a when the characteristic length $\xi_1 = 0.1$.

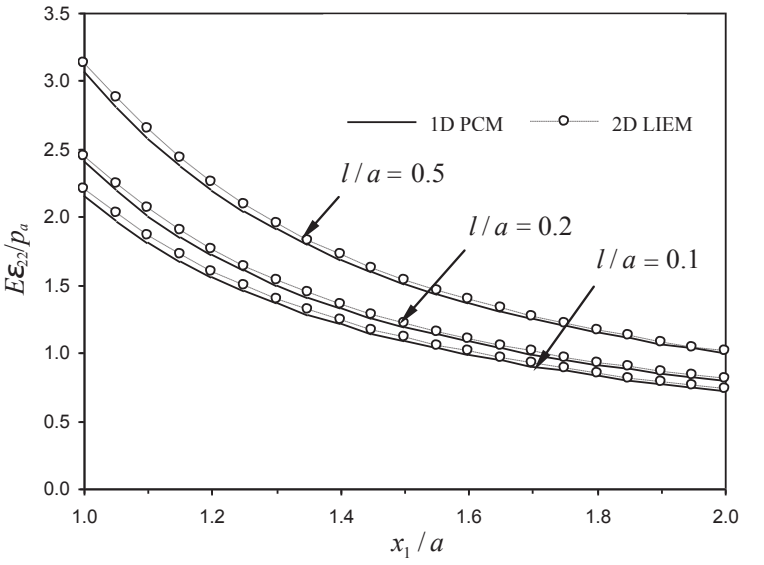

Figure 11: Distribution of the normalized strain $E\varepsilon_{22}/p_a$ for different parameter l/a when the characteristic length $\xi_1 = 0.5$.

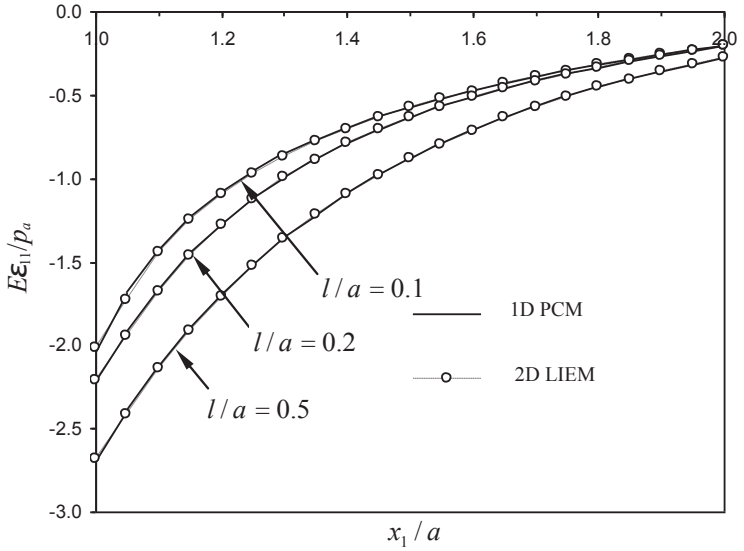

Figure 12: Distribution of the normalized strain $E\varepsilon_{11}/p_a$ for different parameter l/a when the characteristic length $\xi_1 = 0.5$.

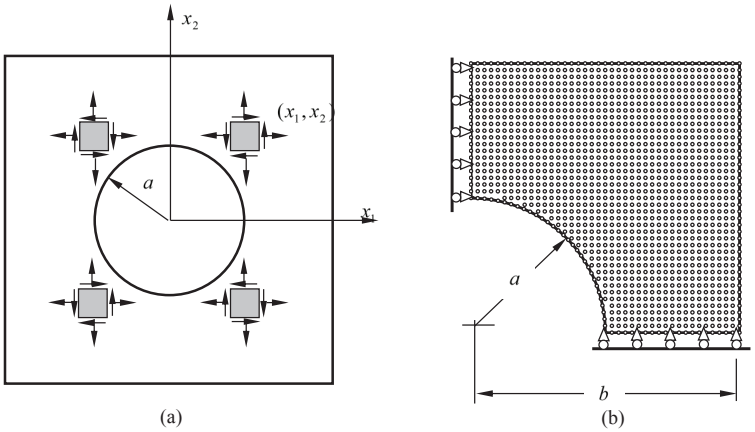

Figure 13: Square plate containing a circle hole under tensile load and quarter of the plate with displacement boundary conditions (a) plate; (b) distribution of node.

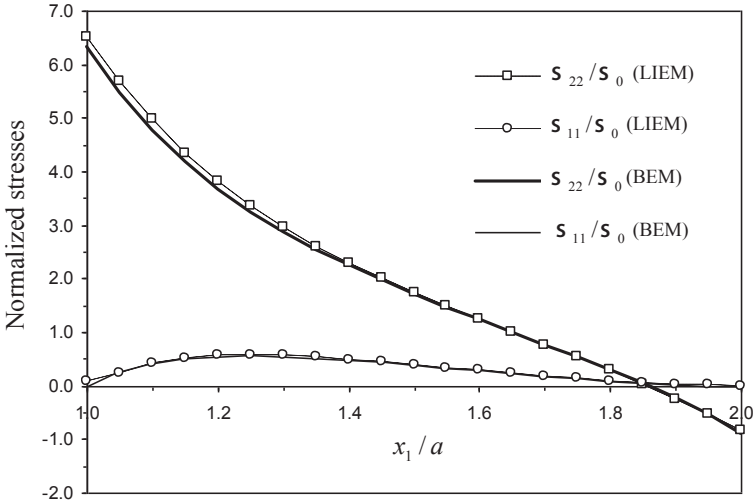

Figure 14: Distribution of the normalized local stresses σ_{11}/σ_0 and σ_{22}/σ_0 along x axis.

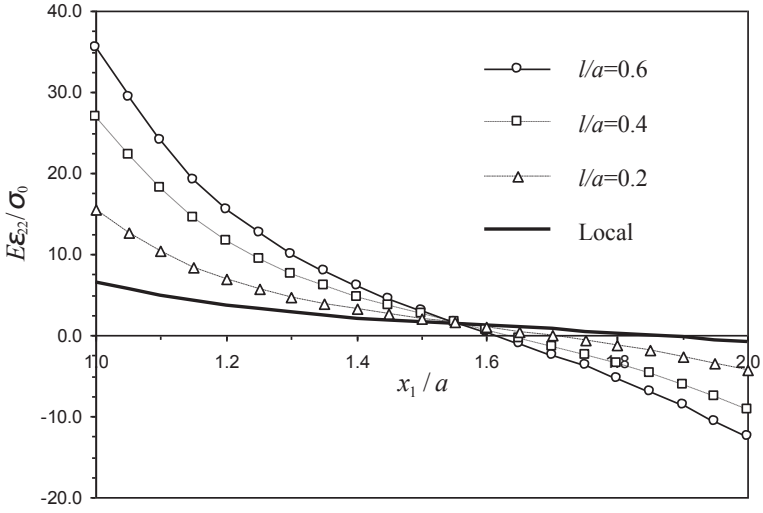

Figure 15: Distribution of the normalized strain $E\varepsilon_{22}/p_a$ for different characteristic length a when the parameter $\xi_1 = 0.1$.

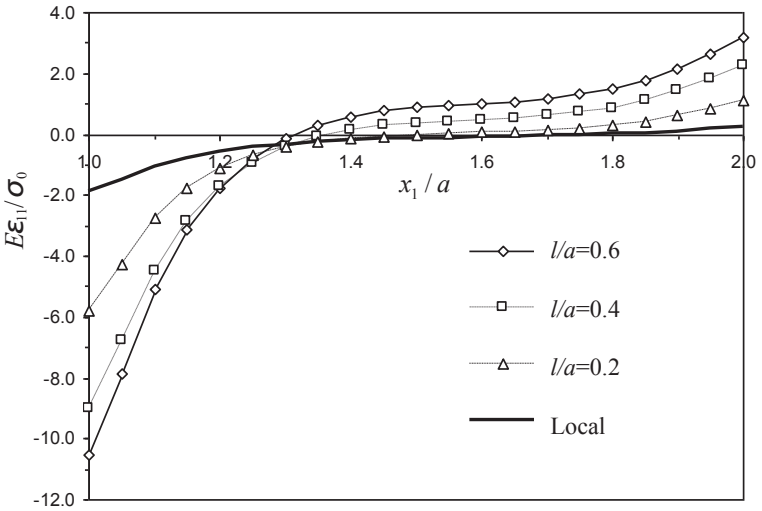

Figure 16: Distribution of the normalized strain $E\varepsilon_{11}/p_a$ for different characteristic length a when the parameter $\xi_1 = 0.1$.

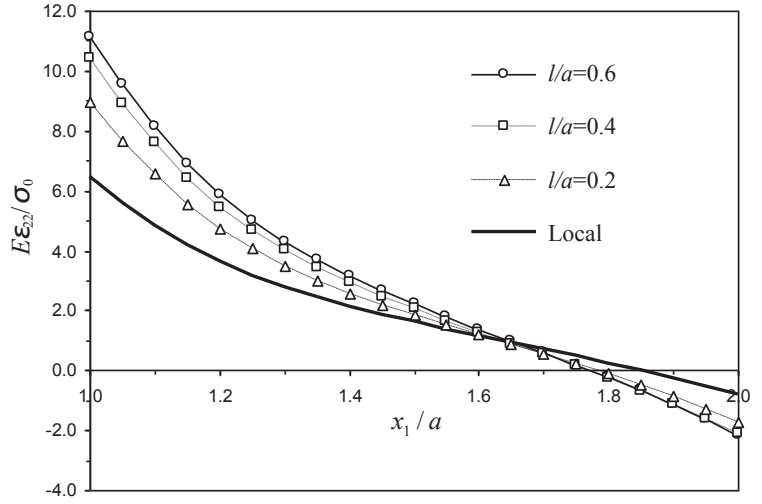

Figure 17: Distribution of the normalized strain $E\varepsilon_{22}/p_a$ for different characteristic length a when the parameter $\xi_1 = 0.5$.

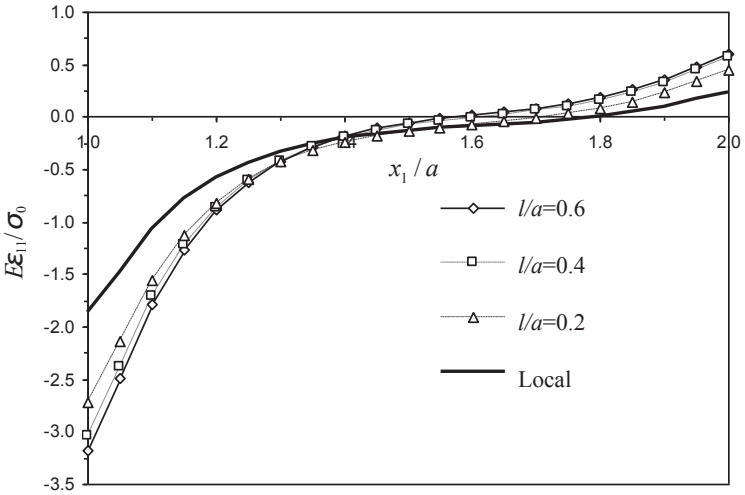

Figure 18: Distribution of the normalized strain $E\varepsilon_{11}/p_a$ for different characteristic length a when the parameter $\xi_1 = 0.5$.

6.3 A square plate with a circle hole under tension

A square plate of width $2b$, containing a circle hole of radius a subjected to a uniform tension σ_0 on the top and bottom is analysed (where $b = 2a$) as shown in Figure 10(a). Same grid of back ground used in the example 6.2 for domain integrals is used and the number of total node is 1364. Due to the symmetry, a quarter of the plate is considered as shown in Figure 10(b). To observe the accuracy of LIEM, the local stresses $(\xi_1 = 1)$ along the axis x_1 is compared with the boundary element method in Figure 16. Good agreement is achieved for both normalized stress σ_{22}/σ_0 and σ_{11}/σ_0. The local $(\xi_1 = 1)$ and nonlocal elastic solutions in terms of strain distribution $E\varepsilon_{11}(x_1,0)/\sigma_0$ and $E\varepsilon_{22}(x_1,0)/\sigma_0$ with different characteristic length (l) for different parameter ξ_1 are plotted in Figures (11) and (12) respectively. It is very clear that for larger value of characteristic length l, the absolute value of the nonlocal strain increases rapidly when the characteristic length increases. For example, from Figure 15, the value of normalized strain $E\varepsilon_{22}(x_1,0)/\sigma_0$ varies from 6.49 (nonlocal) to 35.45 ($l = 0.6a$) at point $(a,\ 0)$, and from -0.825 to -12.53 at point $(b,\ 0)$. As expected, for small value of l, the strain is dominated by the local stress. For the large value of l, this effect by global stresses to strains is increased significantly (see from Figure 14).

7 Conclusions

In this paper, the formulation for the meshless local integral equation method is presented for the nonlocal elasticity analysis. Based on the Eringen's model, a weak form for a set of governing equations with a unit test function is transformed into local integral equations. The meshless method is carried out by using the radial basis functions. Three numerical examples are presented to demonstrate the convergence and accuracy of the proposed method. It is concluded that the meshless local integral equation method is of high accuracy and suitable to deal with 2D nonlocal elasticity problems. As 2D nonlocal elasticity is linear, LIEM can be extended to dynamic case easily using the Laplace transform domain.

References

Altan, S. B. (1989): Existence in Nonlocal Elasticity. *Archive Mechanics*, vol. 41, pp. 25-36.

Atluri, S. N. (2004): *The Meshless Method (MLPG) for Domain and BIE Discretizations*, Forsyth, GA, USA, Tech Science Press.

Barbieri, E.; Meo, M. A. (2011): A Meshless Cohesive Segments Method For Crack Initiation And Propagation In Composites. *Applied Composite Materials*, vol. 18, pp. 45-63.

Bazant, Z. P. (1976): Instability, Ductility and Size Effect in Strain Softening Concrete. *Journal of the Engineering Mechanics Division ASCE*, vol. 12, pp. 331-344.

Bazant, Z. P.; Belytschko, T. B.; Chang, T. P. (1984): Continuum Theory for Strain-softening. *J. Engrg. Mech. Div. ASCE*, vol. 110, pp. 1666-1692.

Bazant, Z. P.; Lin, F. B. (1988): Non-local Yield Degradation. *Int. J. Num. Meth. Engn.*, vol. 26, pp. 1805-1823.

Belytschko, T.; Lu, Y. Y.; Gu, L. (1994): Element-free Galerkin method. *Int. J. Numerical Methods in Engineering*, vol. 37, pp. 229-256.

Eringen, A. C. (1983): On Differential Equations of Nonlocal Elasticity and Solutions of Screw Dislocation and Surface Waves. *J. Appl. Phys.*, vol. 54, pp. 4703-4710.

Eringen, A. C. (1987): Theory of Nonlocal Elasticity and Some Applications. *Res. Mech.*, vol .21, pp. 313-342.

Ferronato, M.; Pini. G. (2010): Finite Element Enrichment Technique by the Meshless Local Petrov-Galerkin method. *Computer Modeling in Engineering & Sciences*, vol. 62, pp. 205-23.

Filiz, S.; Aydogdu, M. (2010): Axial Vibration of Carbon Nanotube Heterojunc-

tions using Nonlocal Elasticity. *Comp Mater Sci,* vol. 49, pp. 619–27.

Hae-Soo, Oh.; Davis, C.; Kim, J-G.; Kwon, Y-H. (2011): Reproducing Polynomial Particle Methods for Boundary Integral Equations. *Computational Mechanics*, vol. 48, no. 1, pp. 1-19.

Hu, Y. G.; Liew, K. M.; Wang, Q.; He, X. Q.; Yakobson, B. I. (2008): Nonlocal Shell Model for Elastic Wave Propagation in Single and Double Walled Carbon Nanotubes. *J Mech Phys Solids*, vol. 56, pp. 3475–85.

Khosravifard, A.; Hematiyan, M.; Marin, L. (2011): Nonlinear Transient Heat Conduction Analysis of Functionally Graded Materials in the Presence of Heat Sources Using An Improved Meshless Radial Point Interpolation Method. *Applied Mathematical Modelling*, vol. 35, pp. 4157-4174

Lazar, M.; Maugin, G. A.; Aifantis, E. C. (2006): On a Theory of Nonlocal Elasticity of bi-Helmholtz Type and Some Applications. *Int. J. Solids and Struct.*, vol. 43, pp. 1404-1421.

Li, L. Y.; Wen, P. H.; Aliabadi, M. H. (2011): Meshfree modelling and homogenization of 3D orthogonal woven composites. *Composites Science and Technology*, vol. 71, pp. 1777-1788.

Li, M.; Hon, Y. C.; Korakianitis, T.; Wen, P. H. (2013): Finite Integration Method for Nonlocal Elastic Bar under Static and Dynamic Loads. *Engineering Analysis with Boundary Elements*, vol. 37, no. 5, pp. 842-849.

Li, S.; Atluri, S. N. (2008): The MLPG mixed collocation method for material orientation and topology optimization of anisotropic solids and structures. *CMES-Computer Modelling in Engineering & Sciences,* vol. 30, pp. 37-56.

Liu, W. K.; Jun, S.; Zhang, Y. (1995): Reproducing Kernel Particle Methods. *Int. J. Numerical Methods in Engineering*,vol. 20, pp. 1081-1106.

Miers, L. S.; Telles, J. C. F. (2006): On the NGF Procedure for LBIE Elastostatic Fracture Mechanics. *Computer Modeling in Engineering & Sciences*, vol. 14, pp. 161-9.

Nayroles, B.; Touzot, G; Villon, P. (1992): Generalizing the Finite Element Method: Diffuse Approximation and Diffuse Elements. *Computational Mechanics,* vol. 10, pp. 307-318.

Pisano, A. A.; Sofi, A.; Fuschi, P.(2009): Nonlocal Integral Elasticity: 2D Finite Element Based Solutions. *Int. J. Solids and Struct.*, vol. 46, pp. 3838-3849.

Sandler, I. S. (1984): *Strain-softening for Static and Dynamic Problems*, in: Proc. Symp. on Constitutive Equations; Micro, Macro and Computational Aspects (ed. K.J. Willam), ASME, New York, pp. 217-231.

Sellountos, E. J.; Polyzos, D.; Atluri, S. N. (2012): A New and Simple Mesh less

LBIE-RBF Numerical Scheme in Linear Elasticity. *CMES-Computer Modelling in Engineering & Sciences*, vol. 89, pp. 513-551.

Sfantos, G. K.; Aliabadi, M. H. (2007): Multi-scale boundary element modelling of material degradation and fracture. *Computer Method in Applied Mechanics and Engineering*, vol. 196, pp. 1310-1329.

Shariati, M. B.; Eslami, M. R.; Hassani, B. (2010): Meshless Analysis of Cracked Functionally Graded Materials Under Thermal Shock. *Mechanika*, vol. 4, pp. 20-7.

Skouras, E. D.; Bourantas, G. C; Loukopoulos, V. C.; Nikiforidis, G. C. (2011): Truly Meshless Localized Type Techniques For The Steady-state Heat Conduction Problems For Isotropic And Functionally Graded Materials. *Engineering Analysis with Boundary Elements*, vol. 35, pp. 452-464.

Sladek, J.; Sladek, V.; Bazant, Z. P. (2003): Non-local Boundary Integral Formulation for Softening Damage. *Int. J. Num. Meth. Engn.*, vol. 57, pp. 103-116.

Sladek, J.; Sladek, V.; Wen, P. H.; Aliabadi, M. H. (2006): Meshless Local Petrov-Galerkin (MLPG) Method for Shear Deformable Shells Analysis. *Computer Modeling in Engineering & Sciences*, vol. 13, pp. 103-17.

Sladek, J.; Stanak, P.; Han, Z-D. et al. (2013): Applications of the MLPG Method in Engineering & Sciences: A Review. *CMES-Computer Modelling in Engineering & Sciences*, vol. 92, pp. 423-475.

Sladek, V.; Sladek, J; Zhang, Ch. (2006): Comparative Study of Meshless Approximations in Local Integral Equation Method. *CMC: Computers, Materials, & Continua*, vol. 4, pp. 177-188.

Sladek, V.; Sladek, J. (2010a): Local Integral Equations Implemented by MLS-approximation and Analytical Integrations. *Engineering Analysis with Boundary Elements*, vol. 34, pp. 904-913.

Sladek, V.; Sladek, J.; Zhang, Ch. (2010b): On Increasing Computational Efficiency of Local Integral Equation Method Combined with Meshless Implementations. *CMES-Computer Modeling in Engineering & Sciences*, vol. 63, pp. 243-263.

Sudak, L. J. (2003): Column Buckling of Multiwalled Carbon Nanotubes using Nonlocal Continuum Mechanics. *J Appl Phys*, vol. 94, pp. 7281–7.

Wang, Q.; Varadan, V. K. (2008): Application of Nonlocal Elastic Shell Theory in Wave Propagation Analysis of Carbon Nanotubes. *Smart Mater Struct*, vol. 16, pp. 178–90.

Wen, P. H.; Aliabadi, M. H. (2009): Evaluation of Mixed-mode Stress Intensity Factors by the Mesh-free Galerkin Method: Static and Dynamic. *Journal of Strain Analysis for Engineering Design*, vol. 44, pp. 273-86.

Wen, P. H.; Aliabadi, M. H. (2007): Meshless Method with Enriched Radial Basis Functions for Fracture Mechanics. *SDHM Structural Durability and Health Monitoring*, vol. 3, pp. 107-119.

Wen, P. H.; Aliabadi, M. H. (2008a): An Improved Meshless Collocation Method for Elastostatic and Elastodynamic Problems. *Communications in Numerical Methods in Engineering*, vol. 24, no. 8, pp. 635-651.

Wen, P. H.; Aliabadi, M. H. (2010): Elastic Moduli of Woven Fabric Composite by Meshless Local Petrov-Galerkin (MLPG) Method. *Computer Modeling in Engineering & Sciences*, vol. 61, pp. 133-54.

Wen, P. H.; Aliabadi, M. H. (2011): A Variational Approach for Evaluation of Stress Intensity Factors using the Element Free Galerkin method. *International Journal of Solids and Structures*, vol. 48, pp. 1171-1179.

Wen, P. H.; Aliabadi, M. H. (2012): Damage mechanics analysis of plain woven fabric composite micromechanical model for mesh-free simulations. *J. Composite Materials*, vol. 46, pp. 2239-2253.

Wen, P. H.; Aliabadi, M. H. (2013): Analytical Formulation of Meshless Local Integral Equation Method. *Applied Mathematical Modelling*, vol. 37, no. 4, pp. 2115-2126.

Wen, P. H.; Aliabadi, M. H.; Liu, Y. (2008b): Meshless Method for Crack Analysis in Functionally Graded Materials with Enriched Radial Base Functions. *Computer Modeling in Engineering & Sciences*, vol. 30, pp. 133-47.

Xiaolin, Li.; Shuling, L. (2011): A Meshless Method for Nonhomogeneous Polyharmonic Problems Using Method of Fundamental Solution Coupled With Quasi-interpolation Technique. *Applied Mathematical Modelling*, vol. 35, pp. 3698-3709.

Zhang, J.; Yao, Z.; Tanaka, M. (2003): The Meshless Regular Hybrid Boundary Node Method for 2D Linear Elasticity. *Engineering Analysis with Boundary Elements*, vol. 27, pp. 259-68.

Zhang, X; Yao, Z.; Zhang, Z.(2006): Application of MLPG in Large Deformation Analysis. *Acta Mechanica Sinica* (English Series), vol. 22, pp. 331-40.